On the resolution and linearity of lensless in situ X-ray beam diagnostics using pixelated sensors

Anton Kachatkou and Roelof van Silfhout*

School of Electrical and Electronic Engineering, Faculty of Engineering and Physical Sciences, University of Manchester, Sackville Street Building, Manchester, M13 9PL, UK
r.vansilfhout@manchester.ac.uk

Abstract: We present a theoretical model that describes the resolution and linearity of a novel transparent X-ray beam imaging and position measurement method. Using a pinhole or coded aperture camera with pixelated area sensors to image a small fraction of radiation scattered by a thin foil placed at oblique angles with respect to the beam, a very precise measurement of the beam position is made. We show that the resolution of the method is determined by incident beam intensity, beam size, camera parameters, sensor pixel size and noise. The model is verified experimentally showing a sub-micrometer resolution over a large linear range.

OCIS codes: (120.3930) Metrology; (170.1630) Coded aperture imaging; (290.5820) Scattering measurements; (340.7440) X-ray imaging; (340.6720) Synchrotron radiation; (350.5730) Resolution.

References and links

1. A. Oed, "Position-sensitive detector with microstrip anode for electron multiplication with gases," Nucl. Instrum. Meth. A **263**(2-3), 351–359 (1988).
2. P. Ilinski, U. Hahn, H. Schulte-Schrepping, and M. Degenhardt, "Residual gas X-ray beam position monitor development for PETRA III," AIP Conf. Proc. **879**, 782–785 (2007).
3. E. D. Johnson and T. Oversluizen, "Compact high flux photon beam position monitor," Rev. Sci. Instrum. **60**(7), 1947–1950 (1989).
4. M. R. Fuchs, K. Holldack, G. Reichardt, and U. Mueller, "Transmissive imaging X-ray beam position monitors (XBPM) for protein crystallography (PX) beamlines," AIP Conf. Proc. **879**, 1006–1009 (2007).
5. T. Martin, G. Baret, F. Lesimple, and P. P. Jobert, "'Semi-transparent' X-ray beam monitor based on nanometric phosphor powder deposited on thin carbon plate," IEEE Trans. Nucl. Sci. **55**(3), 1527–1531 (2008).
6. R. W. Alkire, G. Rosenbaum, and G. Evans, "Design of a vacuum-compatible high-precision monochromatic beam-position monitor for use with synchrotron radiation from 5 to 25 keV," J. Synchrotron Radiat. **7**(2), 61–68 (2000).
7. R. van Silfhout, A. Kachatkou, N. Kyele, P. Scott, T. Martin, and S. Nikitenko, "High-resolution transparent x-ray beam location and imaging," Opt. Lett. **36**(4), 570–572 (2011).
8. N. R. Kyele and R. G. van Silfhout, "Beam Sensing," UK Patent GB2463448 (24 July 2012).
9. P. Revesz, A. B. Temnykh, and A. K. Pauling, "New X-ray scattering-based beam position monitor for high power synchrotron radiation," Nucl. Instrum. Meth. A **621**(1-3), 656–661 (2010).
10. M. Guizar-Sicairos, S. T. Thurman, and J. R. Fienup, "Efficient subpixel image registration algorithms," Opt. Lett. **33**(2), 156–158 (2008).
11. Y. Feng, J. Goree, and B. Liu, "Accurate particle position measurement from images," Rev. Sci. Instrum. **78**(5), 053704–053710 (2007).
12. Q. Tian and M. N. Huhns, "Algorithms for subpixel registration," Comput. Vision Graph. **35**(2), 220–233 (1986).
13. M. R. Shortis, T. A. Clarke, and T. Short, "Comparison of some techniques for the subpixel location of discrete target images," Proc. SPIE **2350**, Videometrics **III**, 239–250 (1994).
14. P. F. I. Scott, A. S. Kachatkou, N. R. Kyele, and R. G. van Silfhout, "Real-time photon beam localization methods using high-resolution imagers and parallel processing using a reconfigurable system," Opt. Eng. **48**(7), 073601–073614 (2009).
15. N. Bobroff, "Position measurement with a resolution and noise-limited instrument," Rev. Sci. Instrum. **57**(6), 1152–1157 (1986).
16. M. Lampton, B. Margon, and S. Bowyer, "Parameter-estimation in X-ray astronomy," Astrophys. J. **208**, 177–190 (1976).

#180505 - $15.00 USD Received 23 Nov 2012; revised 24 Jan 2013; accepted 5 Feb 2013; published 12 Feb 2013

17. F. Zontone, A. Madsen, O. Konovalov, R. Garrett, I. Gentle, K. Nugent, and S. Wilkins, "Measuring the source brilliance at an undulator beamline," AIP Conf. Proc. **1234**, 603–606 (2010).
18. N. M. Allinson, "Development of Non-intensified charge-coupled device area X-ray detectors," J. Synchrotron Radiat. **1**(1), 54–62 (1994).
19. J. R. Janesick, *Photon Transfer: DN->λ* (SPIE Press, Bellingham, Washington, 2007), Chap. 4.
20. F. Zontone, European Synchrotron Radiat Facility, BP 220, F-38043 Grenoble, France (personal communication, 2012). Kapton scattering cross section coefficients: $a_0 = 6.21567 \times 10^{-7}$, $a_1 = -9.62581 \times 10^{-8}$, $a_2 = 7.86926 \times 10^{-9}$, $a_3 = -2.85194 \times 10^{-10}$, $a_4 = 3.78401 \times 10^{-12}$, $b_0 = -6.33669 \times 10^{-8}$, $c_0 = 0.629331$, $d_0 = 3.25478$, $k_0 = 0.110262$, $l_0 = 2.72988$, $b_1 = 7.8529 \times 10^{-9}$, $c_1 = 1.07227$, $d_1 = -294.699$, $k_1 = 0.0543647$, $l_1 = 18.5207$, $C = 21175.44$.
21. B. Lengeler, C. Schroer, J. Tummler, B. Benner, M. Richwin, A. Snigirev, I. Snigireva, and M. Drakopoulos, "Imaging by parabolic refractive lenses in the hard X-ray range," J. Synchrotron Radiat. **6**(6), 1153–1167 (1999).
22. K. J. S. Sawhney, I. P. Dolbnya, M. K. Tiwari, L. Alianelli, S. M. Scott, G. M. Preece, U. K. Pedersen, R. D. Walton, R. Garrett, I. Gentle, K. Nugent, and S. Wilkins, "A test beamline on diamond light source," AIP Conf. Proc. **1234**, 387–390 (2010).
23. R. Ballabriga, M. Campbell, E. Heijne, X. Llopart, L. Tlustos, and W. Wong, "Medipix3: A 64 k pixel detector readout chip working in single photon counting mode with improved spectrometric performance," Nucl. Instrum. Meth. A **633**(Supplement 1), S15–S18 (2011).
24. R. Dinapoli, A. Bergamaschi, B. Henrich, R. Horisberger, I. Johnson, A. Mozzanica, E. Schmid, B. Schmitt, A. Schreiber, X. Shi, and G. Theidel, "EIGER: Next generation single photon counting detector for X-ray applications," Nucl. Instrum. Meth. A **650**(1), 79–83 (2011).
25. E. E. Fenimore, "Coded aperture imaging: predicted performance of uniformly redundant arrays," Appl. Opt. **17**(22), 3562–3570 (1978).
26. K. A. Nugent and B. Luther-Davies, "The use of a regular array of apertures in penumbral imaging," Opt. Commun. **52**(4), 287–291 (1984).

1. Introduction

The availability of diagnostics instruments that measure the position of a probe beam is crucial when the size of a sample becomes similar to the beam cross-section. Also, when a highly focused beam is used to scan larger samples, experimenters must, at all times, be able to assure that no loss of alignment has occurred. It is therefore pivotal to have transparent instruments that measure beam position during experiments and whose output can be used by feedback control schemes to stabilize beam delivery. Existing beam position monitors (BPMs) lack this ability. Ionization chambers [1, 2] have a relatively low spatial resolution. Blade monitors [3] suffer from thermal instability and a relatively small range. Scintillator screens [4, 5] have high absorption at low energies and their efficiency quickly deteriorates with time. Quadrant BPMs based on X-ray fluorescence have a resolution that is limited to 1-2 μm [6]. Recently, we have introduced a method for *in situ* X-ray beam position measurements and imaging which fulfills the aforementioned requirement [7, 8]. A similar measurement scheme has also been described in [9]. The method is based on registering X-ray radiation scattered from a thin foil of a low-Z material with a pinhole or coded aperture camera. The benefits include off-axis detection, a negligible effect on the transmitted beam, flexibility in terms of choice of suitable X-ray detectors, and ability to both perform high-resolution measurements of key beam parameters and produce high quality images of beam cross-section. The off-axis nature of the measurement is of particular interest as it allows us to place the detector system well away from the intense X-ray beam.

By locating the position of the resulting pinhole camera image, a measurement of beam's horizontal and vertical coordinates is made. In the literature, several methods for inferring the exact coordinates of objects as measured by pixelated detectors have been published [10–14]. As such these methods give no indication of the best achievable resolution for a given setup in terms of recorded intensity, object size, detector array pixel size and sensor noise.

In this paper, we provide a detailed mathematical model that describes the resolution of beam position measurements and the linearity of our method. This model equips a user with a tool to maximize instrument resolution. For example, we demonstrate how the use of a dedicated coded aperture rather than a pinhole significantly improves resolution even for relatively weak beam intensities. We compare the results of our model with measurements obtained at the Diamond Light Source (DLS) synchrotron light source.

#180505 - $15.00 USD Received 23 Nov 2012; revised 24 Jan 2013; accepted 5 Feb 2013; published 12 Feb 2013

2. Device model

A diagram of our X-ray beam position monitor (XBPM) is shown in Fig. 1. A negligible part of the incident beam is scattered by a thin amorphous sheet of a low-Z material in all directions allowing us to form an enlarged image of the footprint of the incident beam using a pinhole camera placed underneath the foil.

The center of the recorded image is a representative measure of the beam position along the horizontal (*X*-axis) and vertical (*Z*-axis) directions. If we assume that the sensor is set up so that its sides are parallel to the *X*- and *Y*-axes, the respective coordinates of the image center u_c and v_c can be inferred from two image profiles obtained by summing image rows and columns respectively. Reducing 2D image data to two 1D profiles improves the measured signal-to-noise ratio (SNR) and significantly simplifies and speeds up subsequent signal processing. Each image profile is fitted to a Gaussian function whose center gives the corresponding coordinate of the image position. After the image position is determined, it can be related to the actual beam position if the geometry of the XBPM device is known.

In a typical XBPM application, the user is interested in keeping the beam in a pre-defined, or 'golden', position. By detecting any deviation from that position, compensating control signals can be generated and used to drive appropriate actuators in order to return the beam to the 'golden' position. In the following sections, we therefore mostly focus on investigating the linearity and resolution of beam displacement measurements that can be achieved with our instrument.

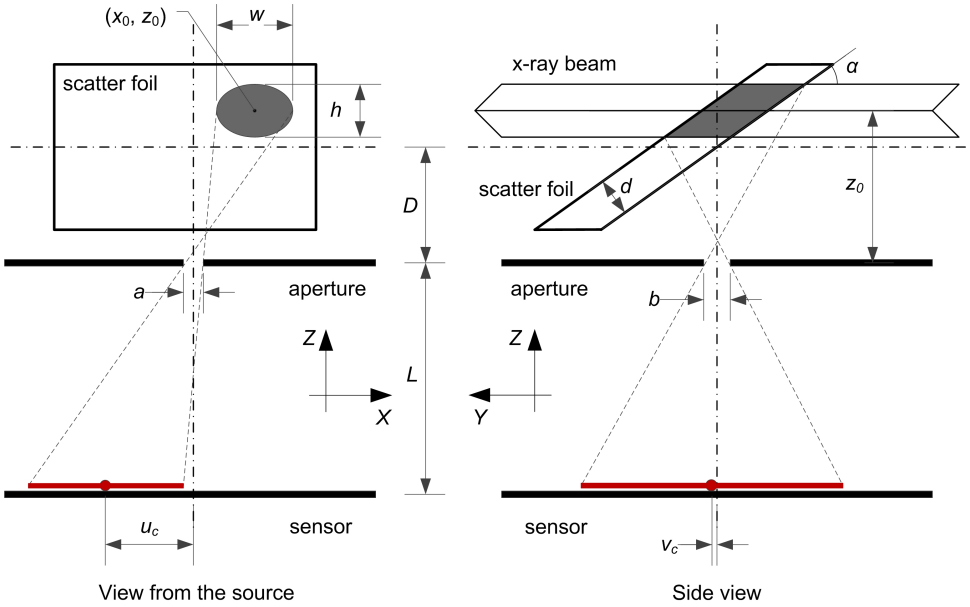

Fig. 1. Beam view and side view of the beam position monitor (not to scale) showing key parameters of the setup used in our model. A pinhole camera collects the X-ray radiation scattered from the highlighted area of the foil (footprint of the beam) and forms a magnified image at the sensor. A measurement of (u_c, v_c) is representative of the beam position (x_0, z_0).

2.1 Linearity

Before discussing the resolution of our device, we first investigate its expected behavior in terms of linearity. Let an X-ray beam with width *w* and height *h* propagate along the *Y*-axis of the Cartesian coordinate system whose origin is at the center of the aperture (Fig. 1). The beam passes through the foil of thickness *d* so that the center of its footprint on the front face of the foil has coordinates (x_0, y_0, z_0). Due to the foil tilt, the *Y*- and *Z*- coordinates of the

#180505 - $15.00 USD Received 23 Nov 2012; revised 24 Jan 2013; accepted 5 Feb 2013; published 12 Feb 2013

footprint are linearly coupled: $z = -y\tan\alpha + D$, where α is the foil tilt angle and D is the distance between the foil and the aperture. We can therefore omit the Y-coordinate when describing beam position, *e.g.* the beam center is located at point (x_0, z_0). The radiation scattered from the foil passes through the aperture and creates an image in the sensor plane at distance L below the aperture plane. We assume that the aperture can have any shape that exhibits symmetry relative to the X- and Y-axes (*e.g.* circular, square, rectangular).

The geometrical center of the image of the footprint as recorded by the sensor, *i.e.* the coordinates of the center of its orthogonal projections to the X- and Y-axes (u_c and v_c respectively), is determined by

$$\begin{aligned} u_c &= -\frac{L}{z_0}x_0 \\ v_c &= -\frac{L}{\tan\alpha}\left(\frac{D+\frac{d}{2\cos\alpha}}{z_0}-1\right). \end{aligned} \tag{1}$$

Here, we assume that the beam is kept near the center of the foil so that z_0 is close to $D + d/(2\cos\alpha)$. Also, due to the geometry of the actual device, D is at least a factor of 10 larger than h, d and b (*e.g.* $D \approx 5$ mm, $h \le 0.5$ mm, $b \le 0.5$ mm and $d \le 0.125$ mm).

Using Eq. (1), it can be shown that small beam movements ($x_0 + \Delta x$, $z_0 + \Delta z$) are readily measured from shifts in position of the recorded image (Δu, Δv):

$$\begin{aligned} \Delta x &= -\frac{D+\frac{d}{2\cos\alpha}}{L}\Delta u \\ \Delta z &= \frac{\tan\alpha\left(D+\frac{d}{2\cos\alpha}\right)}{L}\Delta v \end{aligned}. \tag{2}$$

Thus the proposed XBPM device exhibits a linear response to small beam position fluctuations. Note that any movement in the vertical direction achieves an extra magnification due to the foil tilt. For an infinitesimally thin scatter foil ($d \approx 0$), Eq. (2) reproduces the result given in [7].

2.2 Resolution

The XBPM resolution is determined by the smallest beam position fluctuation (beam displacement or movement) that can reliably be detected by the instrument. The ability of the instrument to measure small beam movements is limited by errors in beam position measurements introduced due to fundamental photon shot noise, and by the instrument itself. We therefore take the resolution to be equal to the standard deviation of beam displacement measurements when all beam parameters, such as position, shape, size and intensity, are kept constant.

Let σ_u and σ_v be the statistical errors of measuring the image X- and Y-coordinates u_c and v_c respectively, and assume that σ_u and σ_v do not depend on u_c and v_c. Then, by applying the uncertainty propagation rules to Eq. (2), the errors in beam displacement measurements along the horizontal, $\sigma_{\Delta x}$, and vertical, $\sigma_{\Delta z}$, directions are expressed via σ_u and σ_v:

#180505 - $15.00 USD Received 23 Nov 2012; revised 24 Jan 2013; accepted 5 Feb 2013; published 12 Feb 2013

$$\sigma_{\Delta x} = \sqrt{2}\,\frac{D + \dfrac{d}{2\cos\alpha}}{L}\,\sigma_u \qquad \sigma_{\Delta z} = \sqrt{2}\tan\alpha\,\frac{D + \dfrac{d}{2\cos\alpha}}{L}\,\sigma_v \tag{3}$$

Here, a $\sqrt{2}$ multiplier accounts for the error increase due to coordinates subtraction when image shift (Δu, Δv) is calculated.

For the given signal-to-noise ratio (SNR) of the image profiles data and the size of sensor, pixel and beam respectively, the quantities σ_u and σ_v can be estimated using a method outlined in [15], which considers χ^2 statistics of the difference between the model instrument response and the observed data.

Let $M \times N$ be the sensor array size, δ_p be the pixel size and assume that the beam image is formed using a circular aperture so that the intensity distribution across the image can be represented by a 2D Gaussian function (see Appendix for the discussion of the validity of the Gaussian approximation). For the profile of the image taken in the *Y*-direction by summing all columns of the pixel array we get:

$$R(v) = MB + A_v e^{-\frac{(v-v_c)^2}{2\Gamma_v^2}}, \tag{4}$$

where B is the pixel background value, A_v is the Gaussian peak amplitude and Γ_v is the Gaussian width representative of the beam height, h, as described in Appendix. Following the procedure outlined in [15], it can be shown that the standard deviation of coordinate measurements is estimated by

$$\sigma_v = \Gamma_v \left(\frac{\Delta_{\chi^2}}{A_v^2 N_{\Gamma_v} tF_v(t)} \right)^{\frac{1}{2}}, \tag{5}$$

where Δ_{χ^2} describes the maximum variation of χ^2 for a given confidence level and in our case (four parameter fit, "1σ" confidence level) is equal to a numeric value of 4.7 [15, 16], N_{Γ_v} is the number of pixels per length Γ_v, and $tF_v(t)$ is an integral term which includes the noise in the measured signal, the image profile parameters and sensor size and sampling rate

$$tF_v(t) = \int_{-t}^{t} \frac{\xi^2 e^{-\xi^2}}{M\left(B + \sigma_r^2\right) + A_v e^{-\frac{\xi^2}{2}}}\, d\xi. \tag{6}$$

Here, $t = N\delta_p/(2\Gamma_v)$ is the parameter describing which fraction of the image profile is measured by the sensor. From inspection of Eq. (5) and Eq. (6), it is clear that for the highest resolution (*i.e.* lowest value of σ_v) one should choose the magnification such that the beam image entirely fits in the active area of the sensor. The integrand's denominator in Eq. (6) describes the contribution of sensor shot and read noise. Equations similar to Eq. (4) – Eq. (6) are readily obtained for σ_u by evaluating the measured beam profile along the *X*-axis.

For a 2D Gaussian, the amplitude A_v, as presented in Eq. (5), is a function of the integrated intensity I_{int}:

$$A_v = \frac{I_{int}}{\sqrt{2\pi} N_{\Gamma_v}}. \tag{7}$$

#180505 - $15.00 USD Received 23 Nov 2012; revised 24 Jan 2013; accepted 5 Feb 2013; published 12 Feb 2013

I_{int} is a function of the flux and energy of the X-ray beam, detector response, the material and thickness of the scatter foil, and the solid angle subtended by the aperture of the pinhole camera. Details of the procedure that we have used to calculate I_{int} are given in the experimental section. Finally, we arrive at the error in image coordinate measurements:

$$\sigma_v = \frac{\Gamma_v}{I_{int}} \left(\frac{2\pi\Delta_{\chi^2} N_{\Gamma_v}}{tF_v(t)} \right)^{\frac{1}{2}}. \tag{8}$$

The resolution of beam movement measurements $\sigma_{\Delta z}$ is determined by the combined effect of Eq. (8) and the terms preceding σ_v in the right-hand part of the corresponding equation in Eq. (3). These terms, which we collectively refer to as a resolution factor, are a function of the pinhole camera magnification. Figure 2 shows how σ_v and the corresponding resolution factor change with respect to the pinhole camera magnification. Point-by-point multiplication of these curves gives the resolution of beam displacement measurements as shown in the inset of Fig. 2. This resolution curve has a distinct minimum that marks the optimal pinhole camera magnification for a given set of XBPM and beam parameters. The magnification at which the minimum occurs mostly depends on the slope of the image position resolution curve and, therefore, largely determined by the integrated intensity of the scattered radiation registered by the detector, I_{int} (see Eq. (8)).

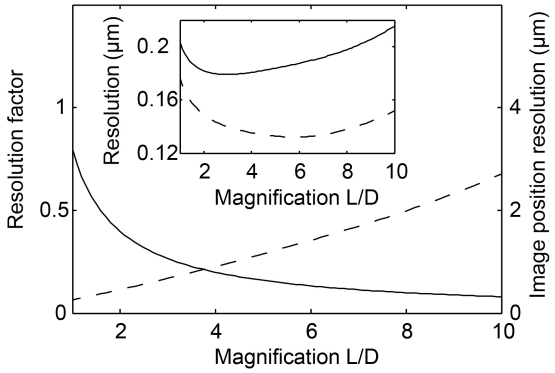

Fig. 2. Resolution factor (solid line) and resolution of image position measurements σ_v (dashed line) as a function of camera magnification for the CMOS indirect detection X-ray area sensor used in our experiments. Their combined effect determines the resolution of beam displacement measurements (solid line in the inset). Model parameters: α = 29°, I_{int} = 10^7 arbitrary digital units (adu), D = 5 mm, d = 125 μm, 200 × 200 μm^2 beam size (as defined by slits), pinhole diameter 500 μm. The dashed line in the inset shows the effect of a "noiseless" detector (see the discussion section).

When I_{int} increases, the minimum moves towards higher magnification values up to the certain value for which the beam image size becomes equal or larger than the detector. In this case, the gain in resolution due to higher magnification is negated by decreasing values of t in the integral term $tF_v(t)$. On the other hand, the lower I_{int}, the lower is the optimal magnification, so that for a particularly weak signal the device has to be operated at the lowest attainable, and often suboptimal, magnification. The optimal magnification can be different for X- and Y- image directions due to the effect of the foil tilt and thickness and differing detector and pixel sizes along these directions.

The above observations regarding the inverse proportional relation between the resolution and integrated intensity has prompted us to consider the use of a special variant of a coded aperture in the form of a ' + ' or crossed slit shape instead of a regular pinhole. When the cross shaped aperture is carefully aligned with the rows and columns of the image sensor, such a coded aperture significantly increases the recorded amplitude A_u (and integrated intensity I_{int}),

#180505 - $15.00 USD Received 23 Nov 2012; revised 24 Jan 2013; accepted 5 Feb 2013; published 12 Feb 2013

without creating an enlarged image (*i.e.* $\Gamma_v = const$) and the usual complication of having to de-convolve the recorded image in order to find a beam position.

3. Experiments

The instrument was tested in a series of experiments at DLS bending magnet beamline B16. A monochromatic beam of 15 keV (after passing through 1 × 1 mm^2 slits) was focused on a stretched Kapton scatter foil by a parabolic compound refractive lens (CRL) down to approximately 11.8 × 11.8 μm^2 full width at half maximum (FWHM).

The linearity of our measurement method (see Eq. (2)) was checked by deliberately scanning a prototype XBPM device across the X-ray beam using a calibrated stage and comparing the measured beam position changes with the set values. The position of the XBPM relative to the incident beam was changed in equal steps, first in vertical and then in horizontal directions. The respective step values were 20 μm and 40 μm whilst the pinhole camera magnification, L/D, was set to 2. Figure 3 shows the difference between the measured beam displacement and the actual motorized stage movement relative to a central position. The resolution of the motorized stage was better than 1 μm.

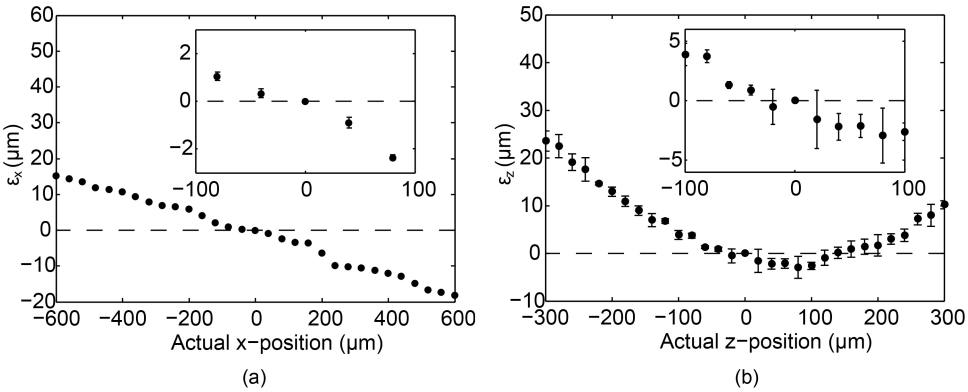

Fig. 3. Difference between measured and actual beam displacements, ε_x and ε_z, at various beam positions in *X*- (a) and *Z*- (b) directions respectively. Beam displacement is derived from image displacement using Eq. (2). The error bars in (a) are comparable or less than the size of the markers. The insets show the near-zero region for both directions. Kapton foil thickness d = 125 μm, tilt angle $\alpha = 21°$, cross aperture with slit width 100 μm, other XBPM parameters are as defined in the text.

For the first set of experiments that investigated the achievable resolution for beamline B16, we used a cross-shaped aperture with a slit width of 200 μm and length of 3 mm. The distance between the foil and the aperture, D, was set to 5 mm, the foil thickness $d = 25$ μm and the foil tilt angle $\alpha = 29°$. The detector was set in different positions to obtain L values ranging from 10 up to 35 mm with a 5 mm step size. For each value of L, several image profiles were taken [14]. The measured image profiles were fitted with a Gaussian curve to determine image position. The standard deviation values of image position measurements were calculated for each L. The obtained values were then converted to the standard deviation of the beam displacement measurements according to Eq. (3). The results for the resolution in the horizontal direction are shown in Fig. 4. We have primarily focused on collecting data regarding the horizontal resolution of the device because the beam was found to be more stable in the horizontal than in the vertical plane.

#180505 - $15.00 USD Received 23 Nov 2012; revised 24 Jan 2013; accepted 5 Feb 2013; published 12 Feb 2013

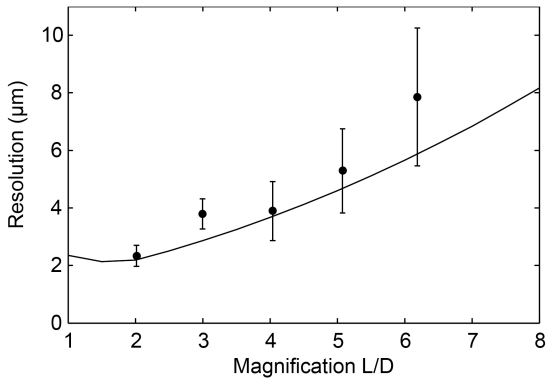

Fig. 4. Resolution of horizontal beam displacement measurements for our instrument as measured at bending magnet beamline B16. Circles correspond to the measured data points, whereas the solid line represents our model for this beamline. XBPM and beam parameters: scatter foil 25 µm thick Kapton tilted at $\alpha = 29°$, photon flux 3×10^{10} photon/s at 15 keV, 11.8 × 11.8 µm^2 FWHM beam focused with Be CRL, cross aperture with slit width 200 µm, detector integration time 1 sec.

For comparison, we calculated the expected resolution values for each detector position using Eq. (5)–Eq. (8) (solid line in Fig. 4). The integrated intensity, I_{int}, was calculated under the assumption that, first, the sensor is large enough and, second, there is no scattering in the medium between the foil and the detector. Hence, all X-ray photons scattered within a solid angle $\Delta\Omega$ subtended by the aperture at any scattering point within the foil contribute into the image:

$$I_{int} = \Phi \cdot \sigma_{scat} \frac{d}{\sin\alpha} \Delta\Omega \frac{DEQ}{K_{ADC}} T_{int}. \tag{9}$$

Here, both the incident flux Φ and the Kapton scattering cross section σ_{scat} depend on X-ray energy, E [17]; DEQ is the sensor's detective quantum efficiency [18], K_{ADC} is its interacting photon to analogue-to-digital converter (ADC) sensitivity [19], and T_{int} is the detector integration or counting time. For all our experiments we used a 1024 × 1280 CMOS image sensor with 7 µm square pixel that was fiber-optically coupled to a Gd_2O_2S:Tb scintillator. The measured pixel read noise was found to be $\sigma_r = 1.74$ adu, $DEQ/K_{ADC} = 2.8$, and the pixel background level was 2.0 adu. The Kapton scattering cross section in the energy range 5 – 25 keV is given by

$$\sigma_{scat} = C\left(\sum_{n=0}^{4} a_n E^n + \sum_{n=0}^{1} b_n \cos\left(\frac{E}{c_n} - d_n\right) e^{-(k_n E) l_n}\right), \tag{10}$$

where E is the photon energy in kiloelectronvolts and a_n, b_n, c_n, d_n, k_n, l_n and C are empirically determined coefficients [20]. The incident flux, Φ, was determined using the estimated flux through the input aperture of the CRL (3×10^{10} photon/sec) and the calculated transmission of the Be CRL (approx. 42.2%) [21]. The estimated incident flux was higher than the value of 2×10^9 photon/sec published in [22] because a double multi-layer monochromator was used in our experiments instead of the standard double crystal monochromator.

Several further experiments to investigate the performance of the device in terms of resolution where conducted in which the thickness of the scatter foil was increased to 125 µm whilst using both cross-shaped apertures of varying size and a pinhole. The foil tilt was lowered to $\alpha = 21°$. The results of our experiments and model calculations are summarized in Table 1.

#180505 - $15.00 USD Received 23 Nov 2012; revised 24 Jan 2013; accepted 5 Feb 2013; published 12 Feb 2013

Table 1. Comparison of calculated and measured resolution of horizontal beam displacement measurements for different aperture shapes and sizes[a]

Magnification *L/D*	Aperture		Calculated resolution (μm)	Measured resolution (μm)
	Shape	Characteristic size (μm)		
2	pinhole	500	2.75	2.58(0)
2	cross	100	0.37	0.42(0)
3	cross	100	0.43	0.49(0)
3	cross	50	0.40	0.35(2)
2	cross	25	0.38	0.31(8)

[a]125 μm Kapton scatter foil, $\alpha = 21°$, detector integration time $T_{int} = 1$ sec; other XBPM and beam parameters are identical to Fig. 4. Aperture characteristic size corresponds to the diameter for circular apertures and the slit width for crosses. The length of slits forming cross apertures is 3 mm.

4. Discussion and conclusion

The XBPM response over the full scan range in Fig. 3 is, to a good approximation, described by Eq. (2). The difference between the measured and actual horizontal displacement shows a calibration (or slope) error that is probably due to a small error in the measurement of the geometry parameters (*e.g.* foil tilt angle α, D and L). In the vertical direction, the residue shows a higher order deviation, which is related to the asymmetry of the setup. The magnification factor changes as the vertical position deviates from the 'golden' position. These deviations are reproducible and can readily be corrected using lookup tables.

Our model provides a clear guide how to optimize the resolution of the proposed device for a given beamline. We have shown that the XBPM resolution is primarily determined by the detector noise, detector pixel size and total integrated intensity. Thus for any given setup a user has several options available to tailor the resolution of the device.

We start our discussion by considering the effect of detector noise. The recent availability of modern hybrid pixel X-ray detectors, which record virtually noiseless images [23, 24], would improve resolution of our device as shown in Fig. 2. The attainable resolution will only be limited by the detector size and practically achievable values for the magnification. The effect of "noiseless" imaging is more profound for low integrated intensities. For example, for $I_{int} = 10^6$ (an order of magnitude lower than in Fig. 2) the resolution will improve by more than a factor of 2. For off-the-shelf charge integrating CMOS and CCD image sensors the effect of background noise on image profiles (see Eq. (4) and Eq. (6)) can be reduced, first, by calculating the profiles for the smallest rectangular region of the sensor that contains the beam image and, second, by discarding profiles' background using an amplitude threshold value chosen as discussed in [15].

The influence of the pixel size on resolution needs careful consideration of Eqs. (5), (7) and (8). By decreasing the pixel size so that the amplitude A_v remains constant, the resolution of spatial measurements will increase in accordance with Eq. (5) due to the improved statistics provided by a higher number of samples of the same signal. This tactic, however, will only work if the total integrated intensity is increased. For the same I_{int} value as the otherwise equivalent detector with larger pixels the resolution will be worse, see Eq. (8).

The most effective and, at the same time, practical way to improve the XBPM resolution is to increase the integrated intensity measured by a given sensor. By considering the parameters in Eq. (9) one readily finds three different ways to achieve higher values of I_{int}. First, the use of either a thicker scatter foil or one made of a higher density material will increase the amount of scattered X-rays. A lower tilt angle also effectively increases the thickness of the foil. Note that both a thicker scatter foil and a lower tilt angle enlarge the recorded image along the tilt direction. Second, the use of apertures with a larger open area increases the solid angle subtended by the sensor ($\Delta\Omega$ term in Eq. (9)). Finally, longer integration or counting times provide a way to increase I_{int} at the expense of lower update rates (lower temporal resolution). In experiments that study dynamic processes, one is interested in highest possible temporal resolution and, therefore, the shortest possible

#180505 - $15.00 USD Received 23 Nov 2012; revised 24 Jan 2013; accepted 5 Feb 2013; published 12 Feb 2013

integration times are desirable. Modern hybrid pixel X-ray detectors are capable of kilohertz frame rates. For high resolution measurements of beam position at such rates, the XBPM device should be configured to maximize the scattered signal that reaches its sensor plane.

The use of apertures with a larger effective area is the preferred option to increase I_{int} because it does not cause larger attenuation of the X-ray beam or slow down the rate at which beam position measurements are made. The use of a traditional circular aperture with a larger diameter is problematic for two reasons. Firstly, a very large aperture would compromise the imaging resolution of the device. Secondly, a larger sensor would be required to accommodate the resulting image at the same magnification setting. The more elegant solution is given by coded apertures. They usually represent an array of relatively small circular apertures arranged in such a way that the amount of light that reaches the detector is maximized while still allowing for high resolution imaging via signal reconstruction [25, 26]. However, the reconstruction step is prohibitively expensive for real-time position measurements. Therefore, we have opted to use a special coded aperture in a shape of two slits crossed at 90° to each other. As mentioned above, when installed in such a way that the slits are parallel to the sides of the sensor, such an aperture provides a significant increase in image intensity while keeping the size of image profiles the same as in the case of the circular aperture with the diameter equal to the width of the slits. The gain in the total measured intensity for this type of aperture exceeds an order of magnitude, as shown in Fig. 5, and is easy to estimate by substituting appropriate solid angle values in Eq. (9).

Figure 5 reveals an interesting property of the cross aperture. There exists an optimal width of the slits that form the cross. It is approximately equal to the size of the beam footprint on the foil and can be explained by some insight into a resolution enhancement mechanism for circular and cross apertures. When the diameter of the circular aperture increases, the extra photons that pass through the larger opening contribute in all image directions so that, when the profiles are calculated, the increased peak intensity is observed. For cross apertures, when the width of the slits increases the extra photons contribute into the image intensity only along the direction across the slit so that, if the beam size in the same direction is smaller than the slit width, the corresponding image profile will broaden while keeping the same peak intensity. As a result, the XBPM resolution will decrease, in accordance with Eq. (5). The optimal slit width for the vertical direction is larger due to the scatter foil tilt and thickness. Note that in order to maximize the resolution boosting effect of the cross aperture we always keep the length of the slits large enough so that their projection matches or exceeds the size of the sensor.

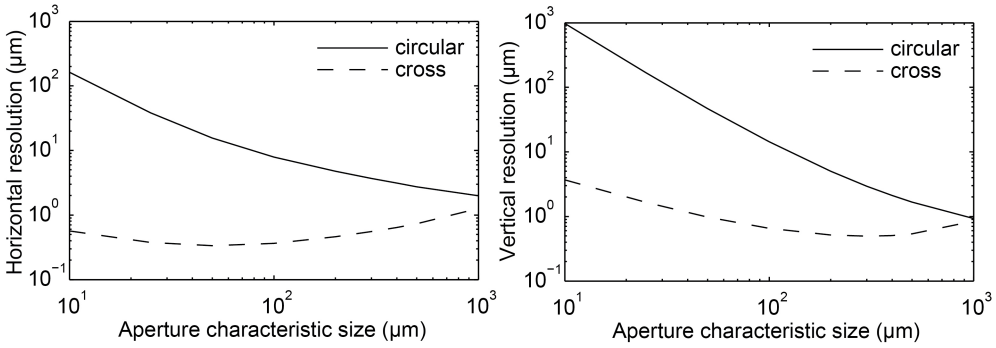

Fig. 5. Comparison of XBPM resolution for two different types of aperture. The XBPM model parameters are the same as in Table 1.

Concluding, we have provided a detailed theoretical description of X-ray beam displacement measurements performed with a pinhole or coded aperture camera that images X-ray radiation scattered from a thin foil. We have shown how the actual change in beam position can readily be obtained from detected changes of the image position using simple

#180505 - $15.00 USD Received 23 Nov 2012; revised 24 Jan 2013; accepted 5 Feb 2013; published 12 Feb 2013

linear equations. Our experiments demonstrate a near linear response of the device particularly for small beam position deviations. The theoretical framework for calculating expected resolution of the device equipped with a foil made of Kapton has also been presented. It can easily be modified for other scattering materials such as CVD diamond, Beryllium and mica foils. With cooled scatter foils the proposed device will be able to achieve excellent resolution figures for the monitoring of white or polychromatic X-ray beams. The fact that the integrated intensity is proportional to the incident X-ray beam flux will have not escaped the attention of the reader.

We have identified the factors that influence device resolution and discussed in detail the most practical ways of improving it. The results of the measurements obtained in experiments with synchrotron radiation are in good agreement with our theory and prove that the proposed device is capable of providing sub-micrometer resolution for incident beam intensities routinely delivered by modern X-ray sources.

Appendix

In synchrotron radiation experiments X-ray beams predominantly have either a Gaussian shape or a top-hat shape. The former is characteristic for focused beams whereas top-hat beams are normally created by cutting a small part of the initial beam with slits. In both cases, due to the superposition of blurring contributions from the scattering foil and the aperture and detector point-spread functions, profiles measured by the XBPM system typically have a bell-like shape. For particularly large top-hat beams or the apertures that are significantly larger than the beam, both profiles have a shape of a bell with a flattened top. A similar shape can also be observed for the vertical profiles obtained for beams whose height is significantly smaller than the thickness of the foil (foil tilt effect). However, in most cases, Gaussian approximation works sufficiently well for reliably determining the position of the profiles. On the other hand, the resolution model presented in this paper can easily be extended to other shapes of profiles (see [15] for discussion), but all the conclusions made in this paper will still be valid.

Gaussian fitting of the image profiles also provides the measure of the image size in the form of two Gaussian width values: one corresponding to beam's height and another to its width. However, it is a non-trivial task to establish a precise relation of these values to the actual beam dimensions. The reason is that part of the information about beam size and shape is lost during profile calculations. In other words, the full image of the scattered signal is required in order to reconstruct the precise shape of the beam and determine its size. However, we have empirically established an approximation which is suitable for estimating the Gaussian width of image profiles that will be registered by the XBPM for a given beam size and vice versa.

Using the same model as in Section 2.1, we can approximate the size of the beam image as $w_u \times w_v$:

$$\begin{aligned} w_u &= a + \frac{L}{z_0}\left(w + a\right) \\ w_v &= b + \frac{bL}{z_0} + \frac{L}{z_0^2 \tan\alpha}\left(\frac{d}{\cos\alpha}\left(z_0 + \frac{h}{2}\right) + hD\right) \end{aligned}. \tag{11}$$

The difference between w_u and w_v and corresponding Gaussian standard deviation values, Γ_u and Γ_v, can be accounted to by using empirically determined coefficients K_w and K_h

#180505 - $15.00 USD Received 23 Nov 2012; revised 24 Jan 2013; accepted 5 Feb 2013; published 12 Feb 2013

$$\Gamma_u = \frac{w_u}{K_w(\varsigma)}$$
$$\Gamma_v = \frac{w_v}{K_h(\varsigma)} \tag{12}$$

whose values are predominantly determined by the number of Gaussian widths, ζ, of the initial X-ray beam with Gaussian intensity distribution that is made visible to the XBPM by upstream slits. Table 2 shows the values of K_w and K_h obtained for different values of ζ.

Table 2. Empirically obtained beam size multiplier values that describe the difference between the measured Gaussian standard deviation of the image profiles and beam image size predicted by Eq. (11)

ζ	K_w	K_h
1	3.95	4.56
2	4.02	4.66
4	4.77	5.03
6	6.23	5.77

Acknowledgment

We would like to thank Kawal Sawhney, Igor Dolbnya and Slava Kachkanov for their help and support during our experiments at B16. This work has been supported financially by EPSRC and has benefitted from earlier proof-of-principle experiments conducted at the DUBBLE CRG beamline BM26A which receives radiation from the European Synchrotron Radiation Facility (ESRF).